

# **A PORE SPACE INVERSION TO ENHANCE RESERVOIR CHARACTERIZATION IN A POROUS DIAGENETIC CARBONATE**

G. N. Boitnott

*New England Research, Inc.*

J. J. Funk

*Saudi Aramco, Lab R&D Center*

## **ABSTRACT**

A suite of eight plugs from a porous diagenetic carbonate reservoir was selected to study the applicability of a new pore structure inversion methodology as a tool to enhance core analysis and log interpretation. Acoustic, flow, and electrical properties were measured on each sample as a function of effective confining pressure. The measured properties were fairly uniform among the suite, exhibiting reasonable first order correlations with porosity. Velocities exhibited more scatter with porosity than did permeability and resistivity. Permeability and formation factor exhibited weak pressure dependence, while velocities exhibited a modest pressure effect.

Based on analysis of thin sections, it is evident that the cores are comprised of a very fine scale pore network with relatively uniform texture. However, due to the fine grained nature of the material, even basic geometrical aspects of the pore geometry are hard to ascertain via optical microscopy. Information about the pore space is limited to NMR size spectra and mercury injection data, which indicate a unimodal distribution of pore sizes and a relatively narrow throat distribution with dominant effective radii slightly less than 1 micron

In order to better define the pore scale interpretation, a pore structure inversion procedure was used to predict pore space models for the cores. The inversions indicate a bimodal throat distribution comprising a fine scale network with characteristic length near 3 microns. Approximately a third of the porosity is estimated to be nodal, with the remaining porosity comprising the throats. Throat shapes and sizes are bimodal, with a dominant population of tubular throats having effective radii slightly less than a micron and a secondary population of crack or slit-like throats with maximum dimension in the range of 3 to 5 microns. Using the inferred pore structures and performing predictions of the various measured quantities (including mercury injection and NMR), we find excellent agreement with experimental observation.

The results provide an interpretation of the core data, suggesting that velocities are influenced by a secondary population of compliant pores that comprise a small fraction of the total porosity. A percolating backbone of less compliant, more tubular throats control the transport properties and allow the compliant throats to be hidden from the throat radii

distributions inferred from mercury injection data. The sub-population of compliant throats is instrumental in creating the short  $T_2$  times observed in these rocks.

## **BACKGROUND**

Thin sections and pore casts were prepared from each sample to provide constraints on pore and network geometry. The pore space in each of the samples was found to be sub-microscopic (pore sizes less than 10 microns). The thin sections show relatively uniform porosity distribution in pores that are not optically resolvable. The pore casts yielded uniform sub-microscopic foams with sub-millimeter size voids representing dissolved patches of dense secondary mineralization with calcite. Both these observations indicate a very fine scale pore network with relatively uniform texture.

NMR  $T_2$  distributions for the suite as a whole are relatively uniform (Figure 1) (see also Funk et. al [2000] for additional details). Unimodal peaks with peak  $T_2$  times ranging from 77 to 242 milliseconds are observed. Comparing NMR spectra and mercury injection data, a surface relaxivity of 2.9  $\mu\text{m/s}$  was inferred for a representative sample as shown in Figure 2. The data support a narrow distribution of sizes as measured with NMR response and an even narrower throat distribution with effective radii slightly less than 1 micron.

Ultrasonic velocities, permeabilities, and electrical properties were measured on each sample as a function of effective confining pressure. Representative data is shown in Figures 3 and 4. The suite was fairly uniform in terms of their measured properties exhibiting reasonable first order correlations with porosity. Velocities exhibit more scatter with porosity than do permeability and resistivity. Permeability and formation factor exhibit weak pressure dependence, while velocities (and dynamic bulk modulus) exhibit a modest pressure effect (Figure 4).

## **PSI: PORE STRUCTURE INVERSION**

A pore space inversion methodology (**PSI**) was used to develop a more refined and physically interpretable framework with which to understand and predict reservoir properties. A flow diagram illustrating the main elements of the **PSI** methodology is shown in Figure 5. Central to the methodology is a set of integrated effective media models which all operate on a generic pore structure shown schematically in Figure 6. The pore space is conceptualized as a heterogeneous network of irregular pores connected by throats of various shapes and dimensions (Figure 6). The fundamental approach of the **PSI** methodology is to objectively determine the possible pore structures which are consistent with observations for a given rock. The constraining data can be any combination of available observations, including a wide variety of core measurements, log measurements, and petrographic observations.

The key advantage of the **PSI** approach is that it produces a three dimensional description of the pore space for each sample which is consistent with all of the known

constraints and is thus directly linked to geophysical properties at the core scale. Another advantage is that the resulting pore space description includes not only the volume fraction and size of nodal pores and vugs, but also the distribution of shapes and sizes of the pore throats. This is done in an internally consistent way, by combining the requirements of all observations into a single pore space model.

## APPLICATION

For this sample set, our knowledge of the pore structure is limited by our inability to image it directly. In the context of this proposed generic pore structure model, there are three parameters that we have very limited constraint on: (1) the characteristic length scale of the network, (2) the amount of nodal porosity, and (3) the mean coordination number of the network.

In an attempt to objectively constrain these parameters while developing a pore space model for the samples, we performed inversions using a range of possibilities for the three unknown parameters: length scale ( $\mathbf{L}$ ), nodal fraction ( $\mathbf{N}$ ), and mean coordination number ( $\mathbf{Z}$ ). Coordination number was found to have little effect on the results. For clarity of explanation, this paper will be limited to results using  $\mathbf{Z}=6$ . Constraints used for the inversions included the measured porosities, permeabilities, resistivities, and dynamic bulk moduli from velocities.

The results of this parameter study are shown in Figure 7. Each set of  $\mathbf{L}$  and  $\mathbf{N}$  for which a solution existed is represented by a square, with the shading of the square being indicative of the "smoothness" or entropy of the pore structure. Regions without a square indicate  $\mathbf{L}, \mathbf{N}$  pairs for which no distribution of throats can be found to fit the constraining data. Therefore this procedure provides indications of the limits on possible length scales and nodal fractions consistent with the constraining data set. Note that pore structures with a wide range of length scales and nodal fractions are possible, each fitting the constraining data set equally well.

The resulting pore structures were then used as inputs into two forward model simulators, one for NMR response and the other for mercury injection. Comparing the simulations with measured data, we find best agreement with the pore structures from inversions using the smaller length scales (see Figure 8). Results from simulations using various nodal fractions at a given length scale tend to produce similar mercury injection and NMR responses, indicating that nodal fraction is not well constrained by the available data set (Figure 9).

While the simulations at short length scales do a reasonable job of predicting mercury injection curves, the predicted models from all of these realizations lead to  $T_2$  distributions with peak times that are consistently too high, indicating that the pore structure inversion process is biasing the results to structures where surface area to volume is too low. To improve the fits the inversions were recomputed with surface area

to volume as an additional constraint, effectively requiring each predicted pore structure to have a specified surface area to volume. By increasing surface area to volume and decreasing length scale, pore structures consistent with the observed  $T_2$  distributions were produced.

The resulting pore structure for one of the samples is shown in Figure 10. The results indicate a bimodal throat distribution in a fine scale network with characteristic length of 3.3 microns. Approximately a third of the porosity is found to be "nodal", with the remaining porosity comprising the throats. Throat shapes and sizes are bimodal, with a strong population of tubular throats with dominant radii slightly less than a micron and a secondary population of crack or slit-like throats with maximum dimension in the range of 3 to 5 microns. Taking these pore structures as inputs to a mercury injection simulator, we find excellent agreement with measured values (Figure 11).

## DISCUSSION

In this paper, we have outlined the use of a pore structure inversion methodology that can be used to develop pore space models of rocks based on core scale geophysical properties. Having constrained a pore space model consistent with all of the observed core scale properties, we are well positioned to develop a physical model for acoustic, NMR, and electrical log properties. It is interesting to note that the predicted pore structures are bimodal in throat shape distribution, while the mercury injection and NMR responses are unimodal. The unimodal nature of the  $T_2$  distribution results from the statistical uniformity of the pore network, while the inferred unimodal nature of the mercury injection data results from the fact that a percolating backbone of tubular throats, with effective radii slightly less than 1 micron, allows the narrower slit like throats to remain hidden (bi-passed) during the injection process.

The inferred pore structures for each of the samples is similar in character, the major differences between samples being the relative amounts of tubular and crack like throats. Subtle variations in these distributions are sufficient to give rise to the observed scatter in velocities and the variations in  $T_2$  times. These variations, being largely controlled by the secondary population of crack like throats, are not resolvable in the transport properties or capillary pressure curves. This interpretation also provides an explanation for why  $T_2$  times are not good predictors of permeability in these samples.

## REFERENCES

- Doyen, P. E., "Crack geometry of igneous rocks: a maximum entropy inversion of elastic and transport properties", *Journal of Geophysical Research* (1987) **92** B8 8169-8181.
- Funk, J. J, S. Siddiqui, M. BaTaweel, and S. Al-Faqeer, "Laboratory techniques to characterize NMR diffusion in carbonates" (2000) *Proceedings SCA 2000* **12** 1-2 .

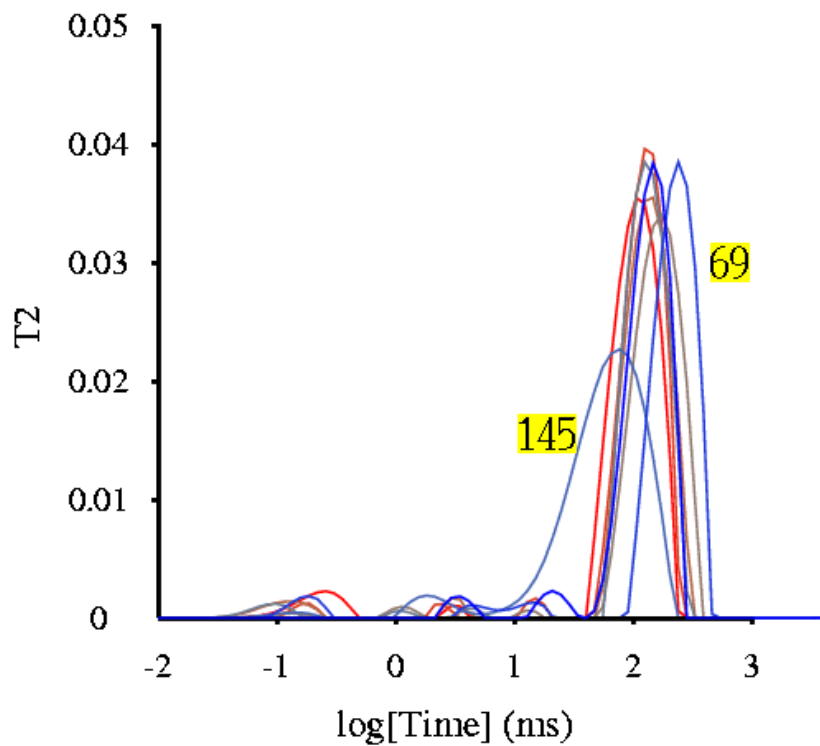


**Figure 1:  $T_2$  distributions for samples studied in this work. Six of the samples had very similar dominant peaks, while two were outliers (145 and 69). Each of the samples exhibited a small but measurable fraction of their response at  $T_2$  times less than 10 ms.**

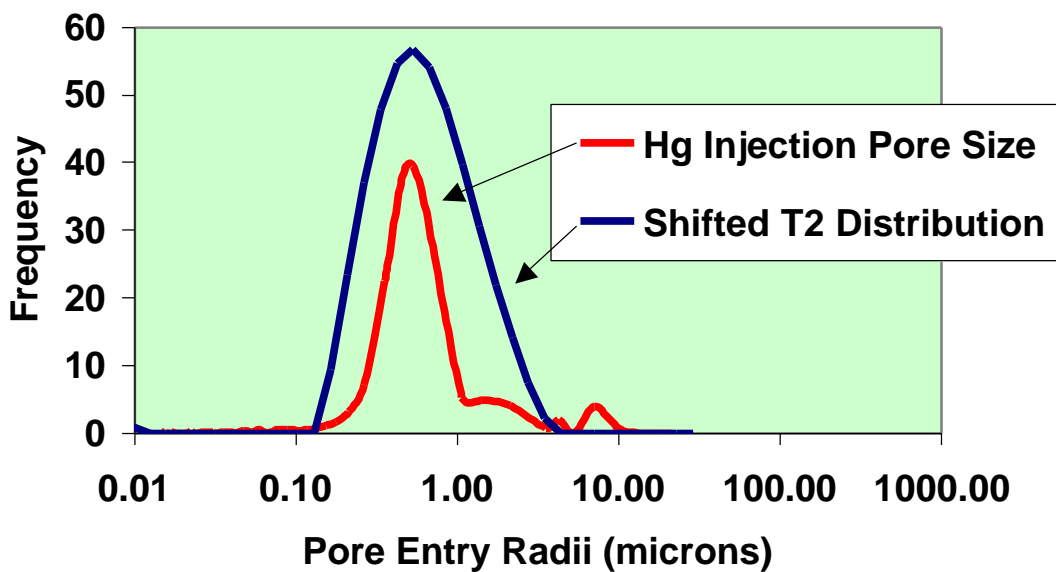


Figure 2: Un-normalized  $T_2$  size and mercury injection size distributions for a representative sample. Both distributions are relatively narrow and dominantly unimodal. The mercury injection data indicates a very narrow distribution of throat sizes with dominant effective radius slightly less than 1 micron. The  $T_2$  distribution is broader in comparison.

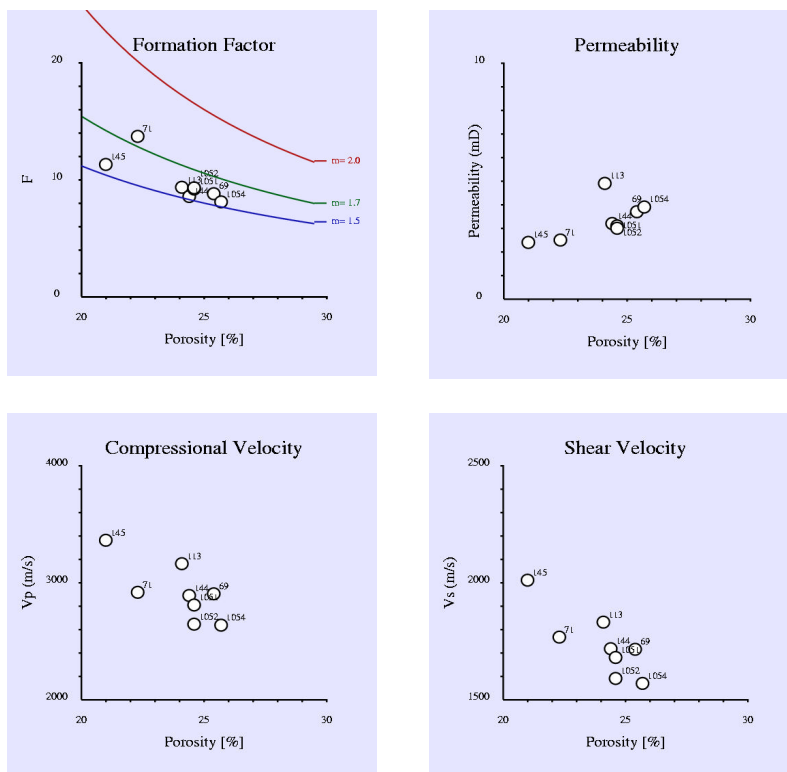


Figure 3: Measured properties of the core samples at 5 MPa effective pressure.

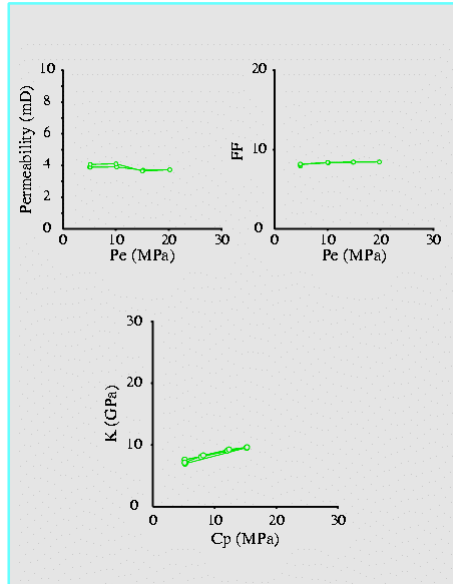


Figure 4: Effect of pressure on the permeability, formation factor (FF) and dynamic bulk modulus (K) of a representative sample. Note the weak pressure dependence of the transport properties in contrast to the modest pressure dependence of the bulk modulus.

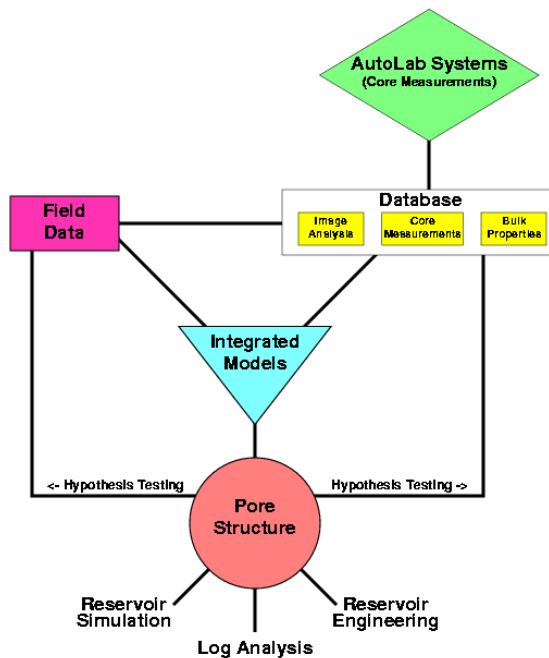
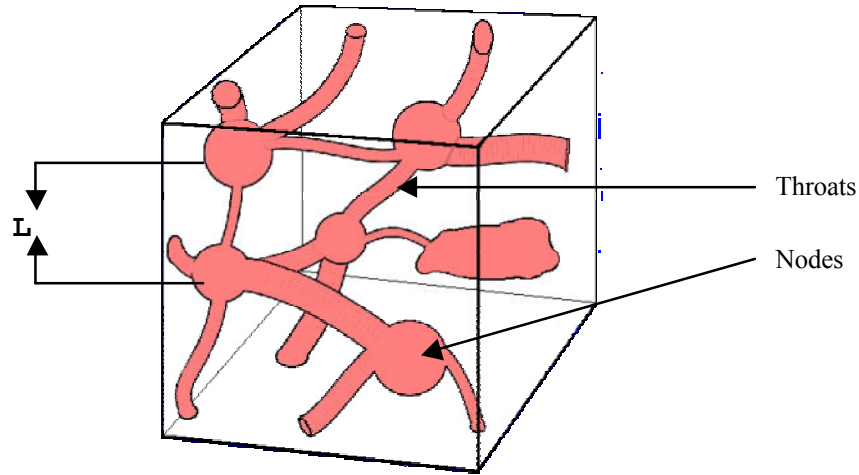
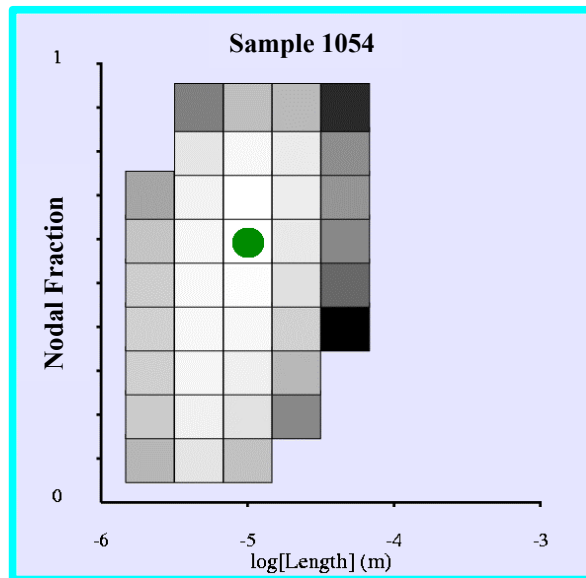


Figure 5: Flow diagram illustrating the PSI pore structure inversion methodology. The theoretical basis for the inversion process is derived from Doyen [1987].



**Figure 6: Conceptual model of the generic pore structure. Pore space is conceptualized as an array of nodal pores connected by a heterogeneous network of throats having varying size and shape. Three geometric parameters define the network: the characteristic length ( $L$ ) which is the mean length between nodes; the nodal fraction ( $N$ ) which is the fraction of porosity tied up in the nodes; and the mean coordination number ( $Z$ ) of the network.**



**Figure 7: Results of the parameter study exploring the possible length scales and nodal fractions consistent with the data. Each box represents a successful inversion, and the shading of each box represents the smoothness or entropy of the pore throat shape spectrum (light shading indicates smooth distributions and dark shading indicates highly structured distributions). The dot indicates the smoothest spectrum, which indicates the length scale and nodal fraction for which the constraining data set was least restrictive.**

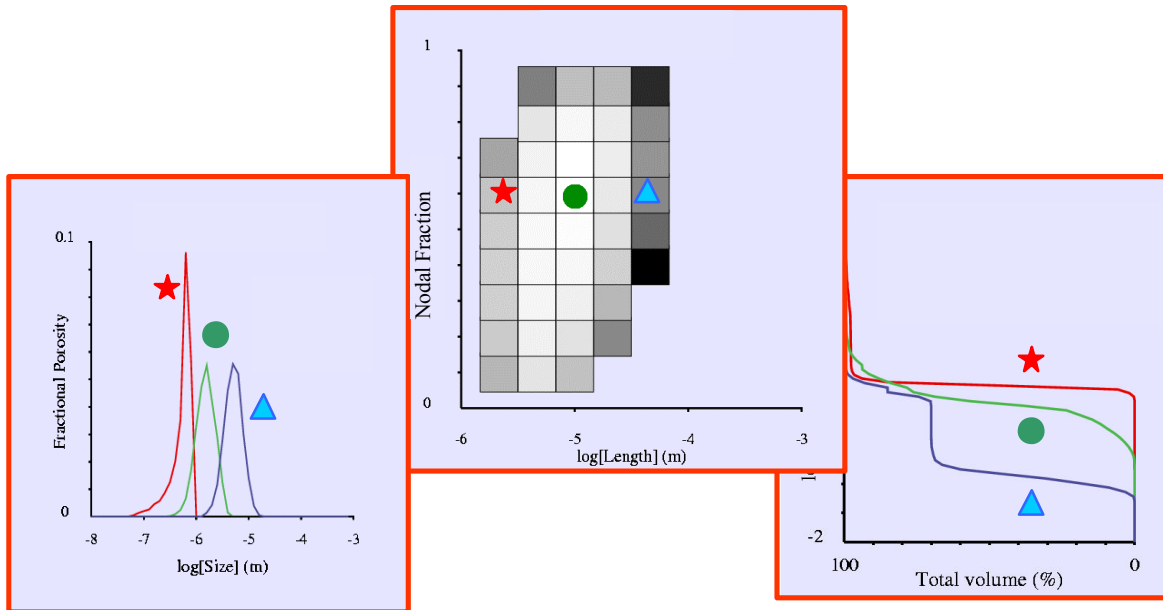


**Figure 8: Forward models of mercury injection (right) and NMR size distribution (left) for selected pore structures with fixed nodal fraction ( $N=0.6$ ) and variable length scale ( $L=2, 10,$  and  $50$  microns). Note that shorter length scale favors narrower throat distributions and smaller size distributions, which are most consistent with measured data.**

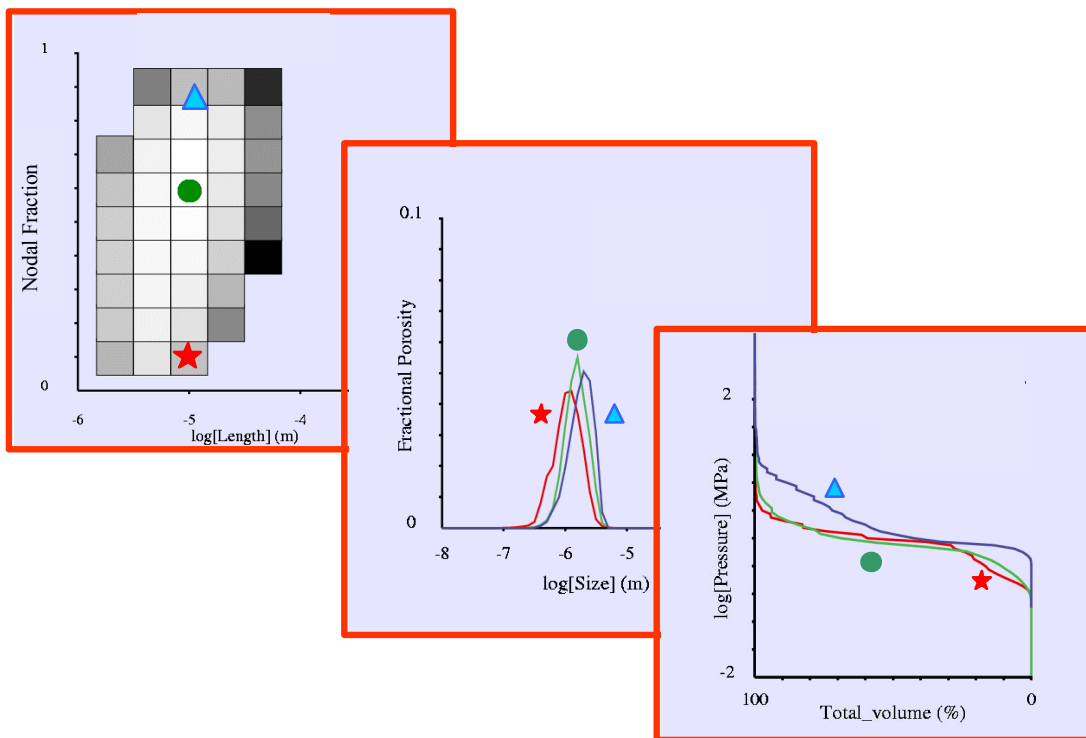


**Figure 9: Forward models of mercury injection (right) and NMR size distributions (center) for selected pore structures with fixed length scale ( $L=10$  microns) but varying nodal fraction ( $N=0.1, 0.6$  and  $0.9$ ). Note that changing nodal fraction does not change the predicted NMR size distribution and only has slight influence on mercury injection response.**

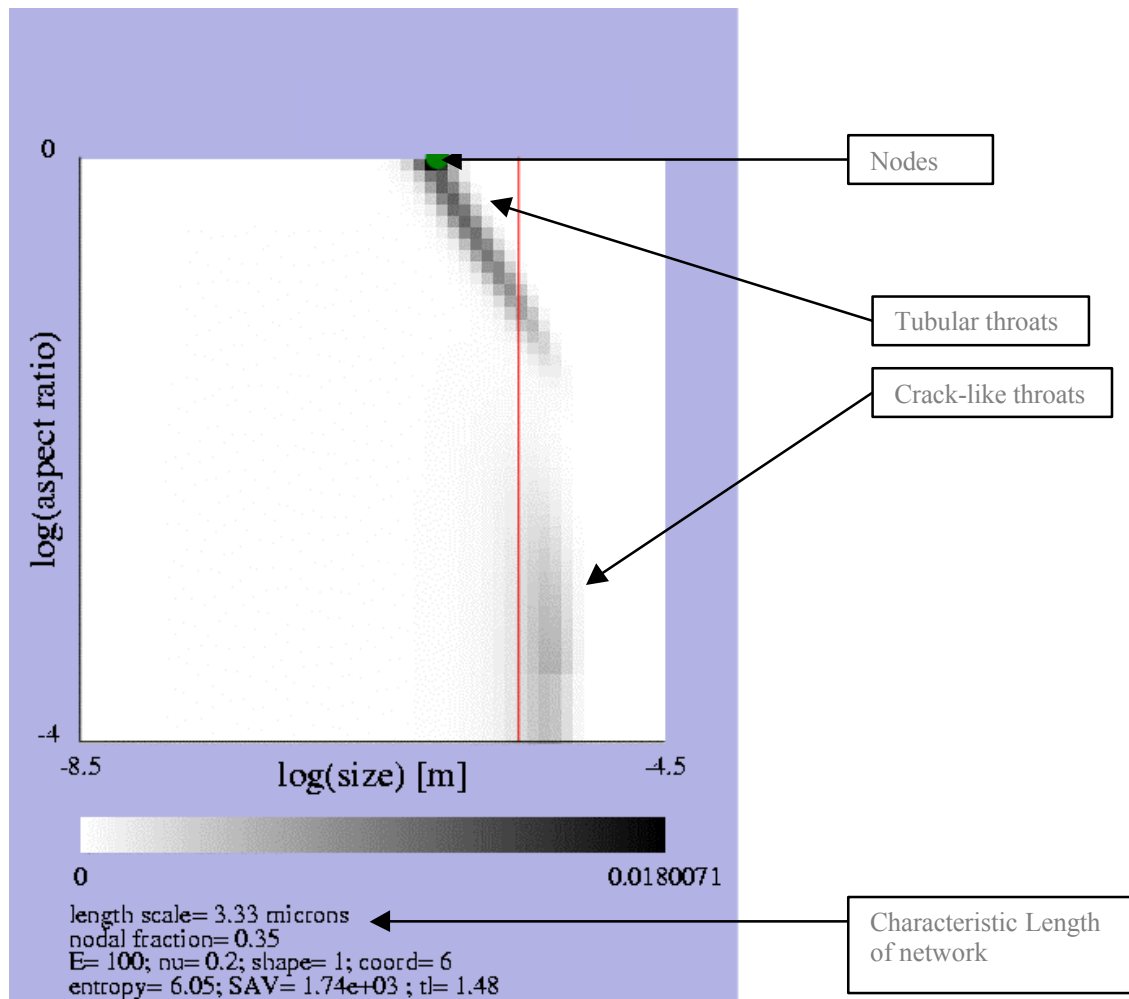


**Figure 10: Pore shape spectrum for sample 1054 based on the measured data in Figure 4 and constraining surface area to volume in order to best fit the measured NMR response. The gray scale graph represents the probability density function of pore throat shapes and sizes which is consistent with the core scale properties used as constraints. The pore throat shape spectrum is bimodal, with a strong concentration of tubular throats (dominant radii less than a micron) and a secondary population of slightly larger crack-like throats.**

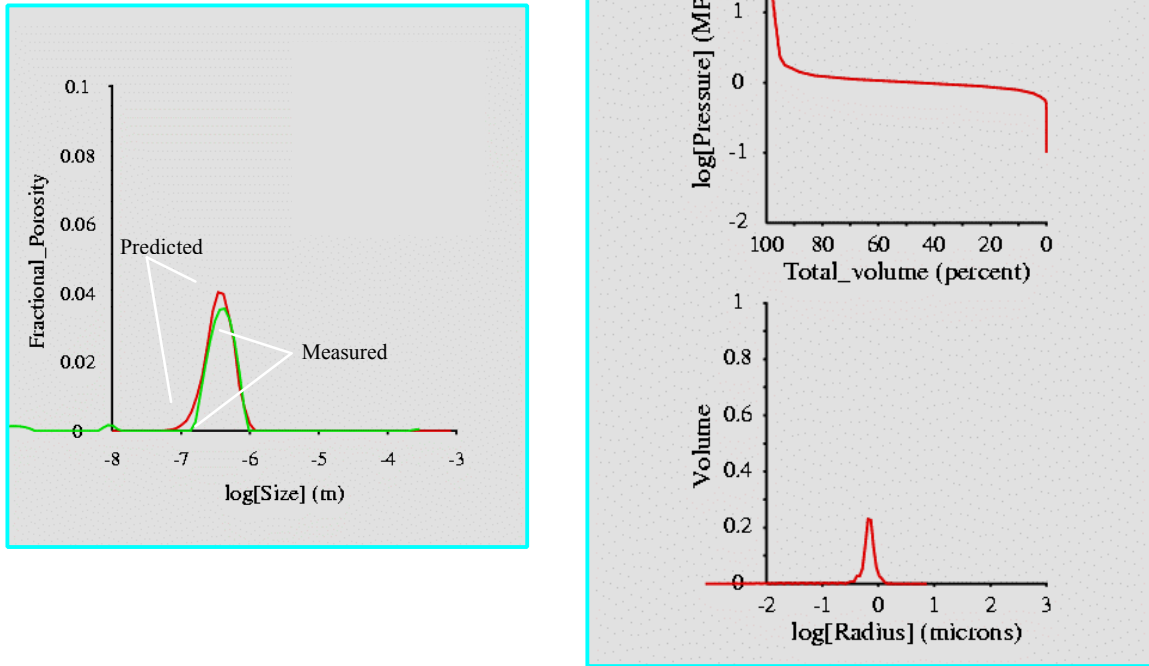


**Figure 11: Predictions using the pore space model of Figure 10. Note the excellent agreement with all of the measured NMR response. The predicted mercury injection response is very similar to that shown in Figure 2 for a similar sample.**